EFFECTS OF PHOTOMETRIC REDSHIFT UNCERTAINTIES ON WEAK LENSING TOMOGRAPHY

Zhaoming Ma[*], Wayne Hu and Dragan Huterer
Kavli Institute for Cosmological Physics and Department of Astronomy & Astrophysics,
University of Chicago, Chicago, IL 60637
Draft version June 24, 2005

ABSTRACT

We perform a general analysis of the effects of photometric redshift uncertainties on weak lensing tomography. We describe the photo-z distribution with a bias and Gaussian scatter that are allowed to vary arbitrarily in redshift. We find that both the bias and the scatter are important, and for a fiducial next-generation survey each would need to be known to better than about $0.003 - 0.01$ in each $\delta z = 0.1$ bin in order to lead to less than a factor of 1.5 increase in the dark energy parameter errors. The more stringent requirement correspond to a larger dark energy parameter space, when redshift variation in the equation of state of dark energy is allowed. Of order $10^4 - 10^5$ galaxies with spectroscopic redshifts will be needed to achieve this level of calibration. These requirements increase in stringency for more ambitious surveys; we quantify such scalings with a convenient fitting formula. No single aspect of a photometrically binned selection of galaxies such as their mean or median suffices, indicating that dark energy parameter determinations are sensitive to the shape and nature of outliers in the photo-z redshift distribution.

Subject headings: cosmology – gravitational lensing, large-scale structure of the universe

1. INTRODUCTION

Weak gravitational lensing of galaxies by large scale structure is rapidly becoming one of the most powerful cosmological probes (Bartelmann & Schneider 2001; Refregier 2003). Following the first detections a few years ago (Van Waerbeke et al. 2000; Kaiser, Wilson & Luppino 2000; Bacon et al. 2000a; Wittman et al. 2000; Refregier et al. 2003), weak lensing has produced increasingly better constraints on the matter density relative to critical Ω_m and the amplitude of mass fluctuations σ_8 (Hoekstra, Yee & Gladders 2002; Pen, van Waerbeke & Mellier 2002; Brown et al. 2003; Jarvis et al. 2003; Pen et al. 2003; Heymans et al. 2005; Van Waerbeke, Mellier & Hoekstra 2005). While weak lensing is most sensitive to the amount and distribution of dark matter, it also has the potential to probe the dark energy through its effect on the growth of structure and distances (Hu & Tegmark 1999; Huterer 2002; Hu 2003; Takada & Jain 2003; Song & Knox 2004; Ishak 2005). Indeed, when combined with other cosmological probes, weak lensing data already produce interesting constraints on the dark energy (Jarvis et al. 2005).

By utilizing source galaxy redshifts to study the growth of structure and the distance-redshift relation tomographically, substantially more dark energy information can be recovered (Hu 1999). In fact future weak lensing surveys such as PanSTARRS[1], Supernova/Acceleration Probe (SNAP[2]; Aldering et al. 2004) and Large Synoptic Survey Telescope (LSST[3]) are expected to impose constraints on dark energy that are comparable to those from type Ia supernovae (see e.g. Refregier et al. 2004). In the more near term, the Canada-France-Hawaii Telescope Legacy Survey (CFHTLS[4]) and the Dark Energy Survey[5] are expected to help bridge the gap between the current and ambitious future surveys.

Powerful future surveys will require a much more stringent control of the systematics. Recent work has addressed systematic errors from the computation of the non-linear power spectrum (White & Vale 2003, 2004; Heitmann et al. 2004; Huterer & Takada 2005; Hagan, Ma & Kravtsov 2005), baryonic cooling and pressure forces on the distribution of large-scale structures (White 2004; Zhan & Knox 2004), approximations in inferring the shear from the maps (Dodelson & Zhang 2005; White 2005), the presence of dust (Vale et al. 2004). Such studies have stimulated work on how to improve the PSF reconstruction (Jarvis & Jain 2004), estimate shear from noisy maps (Bernstein & Jarvis 2002; Hirata & Seljak 2003; Hoekstra 2004), and protect against the small-scale biases in the power spectrum (Huterer & White 2005).

In this work we consider the effect of errors in photometric redshifts of source galaxies on weak lensing tomography. Of course, the total number of galaxies, which is currently in the millions and might be in the billions with future surveys, is too large for spectroscopic measurements to be feasible. One therefore needs to rely on the photometric redshifts whose accuracy, while presently adequate, may not be sufficient for future surveys which are expected to have very small statistical errors. Uncertain photometric redshifts blur the tomographic bin divisions of source galaxies. In the extreme case when photometric redshift errors are comparable to the width of the distribution itself, one completely loses tomographic information degrading the cosmological parameter accuracies by up to an order of magnitude.

In this paper we study how the photometric redshift uncertainties affect cosmological parameter determinations. We construct an explicit mapping between the photometric and true redshifts, and parametrize it to al-

[*]Email: mzm@oddjob.uchicago.edu
[1] http://pan-starrs.ifa.hawaii.edu
[2] http://snap.lbl.gov
[3] http://www.lsst.org
[4] http://www.cfht.hawaii.edu/Science/CFHLS
[5] http://cosmology.astro.uiuc.edu/DES

low an arbitrary redshift dependence of the bias and scatter in this relation. We then study how accurately the photometric redshifts need to be known *a priori* and, in particular, which details of the photometric redshift error distribution are the main source of degeneracy with cosmological parameters. We hope that this study will help stimulate work on assessing and improving existing algorithms for photometric redshift estimation (e.g Cunha et al. 2005).

The outline of the paper is as follows. In §2, we introduce the formalism and parametrizations of both cosmology and photometric redshift errors. We explore the loss of lensing information on the dark energy to photometric redshift uncertainties in §3. We show how this lost information is regained as we impose prior knowledge of the photometric redshift parameters in §4. We discuss our results and conclude in §5.

2. METHODOLOGY

In this section, we discuss the modeling of the photometric redshift distribution. We then illustrate the flexibility of this description through two different fiducial models for the distribution. Finally we discuss its relationship to lensing observables and the Fisher formalism for addressing its impact on parameter estimation.

2.1. *Photo-z Distribution*

Having only the photometric redshift ("photo-z") of the source galaxies at hand, the observer will necessarily bin the galaxies by their photometric redshifts $z_{\rm ph}$ rather than true (spectroscopic) redshifts z. With a probability distribution $p(z_{\rm ph}|z)$ in $z_{\rm ph}$ at a given z, the true redshift distributions of the bins necessarily overlap.

In general this distribution can vary arbitrarily with z. The true distribution of galaxies $n_i(z)$ that fall in the ith photo-z bin with $z_{\rm ph}^{(i)} < z_{\rm ph} < z_{\rm ph}^{(i+1)}$ becomes

$$n_i(z) = \int_{z_{\rm ph}^{(i)}}^{z_{\rm ph}^{(i+1)}} dz_{\rm ph}\, n(z)\, p(z_{\rm ph}|z)\,. \tag{1}$$

$n(z) = d^2N/dzd\Omega$ is the overall galaxy redshift distribution, and is chosen to have the form

$$n(z) \propto z^\alpha \exp\left[-(z/z_0)^\beta\right]\,. \tag{2}$$

Unless otherwise stated we will adopt $\alpha = 2$, $\beta = 2$ and fix z_0 such that median redshift is $z_{\rm med} = 1$. The total number of galaxies per steradian

$$n^A = \int_0^\infty dz n(z)\,, \tag{3}$$

fixes the normalization, and we analogously define

$$n_i^A = \int_0^\infty dz n_i(z) \tag{4}$$

for the bins.

By construction, the sum of the individual distributions equals the total $\sum_i n_i(z) = n(z)$. Therefore, regardless of how complicated the photo-z probability distribution gets and hence the redshift distributions of the tomographic bins, the total distribution of galaxies $n(z)$ is unchanged.

This construction cleanly separates uncertainties due to the photometric redshifts of the individual survey

galaxies characterized by $p(z_{\rm ph}|z)$ from uncertainties in the redshift distribution of the underlying total distribution of galaxies $n(z)$. We mainly consider the former in this work but comment on the latter in §5 (see also Huterer et al. 2005). The rationale is that even without any knowledge of the photo-z's of the survey galaxies themselves, one can at least bin all of the galaxies together assuming that the underlying redshift distribution or selection function of the survey is known. In practice, this means that one must obtain information about the underlying distribution from an independent source (say, another survey through a study of the luminosity function) or from a fair subsample of survey galaxies with spectroscopic redshifts.
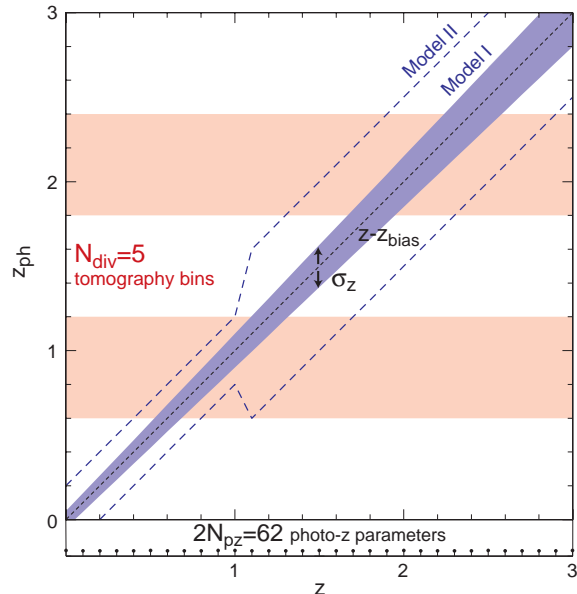

FIG. 1.— Parametrization of the photo-z distribution and two illustrative fiducial models. The distribution spreads galaxies at a given redshift z into a distribution in $z_{\rm ph}$ characterized here by a bias $z_{\rm bias}$ and a scatter σ_z whose evolution is parametrized by interpolating their values at $N_{\rm pz}$ redshifts z_μ. In both models $z_{\rm bias} = 0$, whereas σ_z, given in §2.2, is illustrated here for model I (shaded region) and model II (dashed lines) as 1σ bands. Galaxies binned according to their photometric redshifts ($N_{\rm div}$ horizontal bands) then have overlapping redshift distributions determined by the $2N_{\rm pz}$ photo-z parameters.

2.2. *Photo-z Models*

Any photo-z model may be described by providing a function for the distribution of photometric redshifts given the true redshift, $p(z_{\rm ph}|z)$. For the purposes of this paper we take the simplifying assumption that this function is a Gaussian at each redshift, i.e.

$$p(z_{\rm ph}|z) = \frac{1}{\sqrt{2\pi}\sigma_z} \exp\left[-\frac{(z - z_{\rm ph} - z_{\rm bias})^2}{2\sigma_z^2}\right]\,. \tag{5}$$

However, we allow the bias $z_{\rm bias}(z)$ and scatter $\sigma_z(z)$ to be arbitrary functions of redshift. The redshift distribution of the tomographic bins defined by equation (1) can then be written as

$$n_i(z) = \tfrac{1}{2}n(z)\left[\mathrm{erf}(x_{i+1}) - \mathrm{erf}(x_i)\right], \tag{6}$$

with

$$x_i \equiv (z_{\rm ph}^{(i)} - z + z_{\rm bias})/\sqrt{2}\sigma_z, \tag{7}$$

where $\mathrm{erf}(x)$ is the error function.

The Gaussian assumption is not as restrictive as it might naively seem. By allowing the bias and scatter to be arbitrary functions of redshift one can obtain arbitrarily complex redshift distributions in the tomographic bins through equation (1). In fact, the mapping is in principle completely general for finite bins and a smooth underlying distribution. Galaxies in a finite range of redshift over which the distribution is nearly constant can then be mapped to any z_{ph}.

In practice we will represent the free functions $z_{\mathrm{bias}}(z)$ and $\sigma_z(z)$ with a discrete set of N_{pz} photo-z parameters. They represent the values of the functions at z_μ which are equally spaced from $z = 0$ to 3. To evaluate the functions at an arbitrary redshift, we take a linear interpolation of the discrete parameters in redshift.

While a finite N_{pz} does restrict the form of the distribution, it still allows radically different redshift distributions given the same tomographic bins. For example, consider two different photo-z models

- Model I: $z_{\mathrm{bias}}(z) = 0$; $\sigma_z(z) = 0.05(1 + z)$.

- Model II: $z_{\mathrm{bias}}(z) = 0$; $\sigma_z(z) = 0.2$ for $z < 1.0$ and $\sigma_z(z) = 0.5$ for $z > 1.0$.

The distribution $p(z_{\mathrm{ph}}|z)$ is illustrated in Figure 1 for $N_{\mathrm{pz}} = 31$ through the 1σ scatter region. The resulting redshift distributions for $N_{\mathrm{div}} = 5$ tomographic bins are shown in Figure 2. These specific choices of N_{pz} and N_{div} are motivated in §3.

Model II demonstrates that sharp changes in the Gaussian photometric parameters can map neighboring galaxies in redshift to quite different tomographic bins. The redshift distributions of the bins can thus have features that are sharper than the assumed scatter. Additionally, photo-z degeneracies that take two distinct spectroscopic redshift ranges into a single photometric redshift and lead to bimodality in the binned distribution can be modeled by a large z_{bias}. Thus by allowing this set of parameters to freely vary one can access a wide range of tomographic redshift distributions. Uncertainty in these parameters will then cause uncertainties in tomographic dark energy determinations.

2.3. Lensing Observables

The convergence power spectrum at a fixed multipole ℓ and for the ith and jth tomographic bin $P_{ij}^\kappa(\ell)$ is given by (Kaiser 1992, 1998)

$$n_i^A n_j^A P_{ij}^\kappa(\ell) = \int_0^\infty dz\, W_i(z)\, W_j(z) \frac{H(z)}{D^2(z)}\, P(k_\ell, z)\,, \quad (8)$$

where $H(z)$ is the Hubble parameter, and $D(z)$ is the angular diameter distance in comoving coordinates. $P(k_\ell, z)$ is the three-dimensional matter power spectrum and $k_\ell = \ell/D(z)$ is the wavenumber that projects onto the multipole ℓ at redshift z. The weights W are given by

$$W_i(z) = \frac{3}{2}\, \Omega_m\, \frac{H_0^2 D(z)}{H(z)}(1 + z)$$
$$\times \int_z^\infty dz'\, n_i(z') \frac{D_{LS}(z, z')}{D(z')}\,, \quad (9)$$
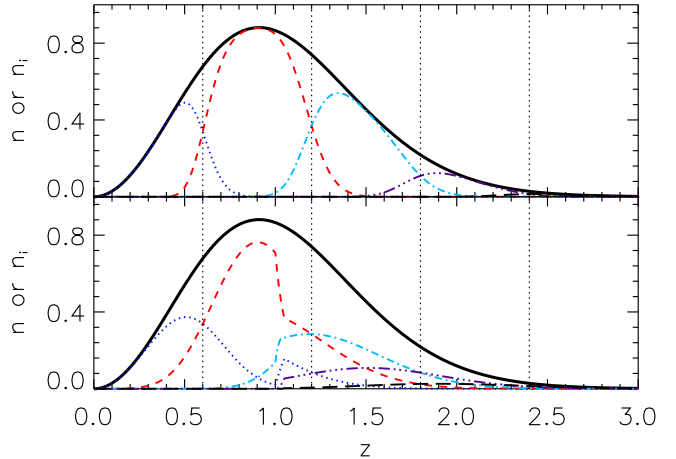

FIG. 2.— Source galaxy redshift distribution $n(z)$. Top panel: photo-z model I. Lower panel: photo-z model II. The solid curve is the overall galaxy distribution defined in equation (2). The other curves are the true (spectroscopic) distributions that correspond to the sharp divisions in photo-z space (denoted by dotted vertical lines).

where $D_{LS}(z, z')$ is the angular diameter distance between the two redshifts. The power spectrum is computed from the transfer function of Eisenstein & Hu (1999) with dark energy modifications from Hu (2002), and the non-linear fitting function of Peacock & Dodds (1996).

With tomographic binning, the number weighted power spectrum $n_i^A n_j^A P_{ij}^\kappa$ and not P_{ij}^κ is the fundamental observable. Even given photometric redshift uncertainties in the binning it is always possible to recover the total weighted power spectrum (Hu 1999)

$$(n^A)^2 P^\kappa = \sum_{i,j=1}^{N_{\mathrm{div}}} n_i^A n_j^A P_{ij}^\kappa\,, \quad (10)$$

since the weighting is based on the observed n_i^A. By treating $n_i^A n_j^A P_{ij}^\kappa$ as the observable one guarantees that the addition of photo-z estimates for the individual galaxies can only add information. This would not be true if P_{ij}^κ were taken as the only observable quantity. Given that changes in photo-z parameters induce changes in n_i^A, the binned power spectra P_{ij}^κ do not contain enough information to weight the power spectra and recover the total P^κ.

That the binned angular number densities n_i^A are observed quantities also implies that there is additional direct information on the photo-z parameters that does not depend on shear measurements. For example, a high fraction of galaxies in bins with z_{ph} larger than the median redshift would imply a large photo-z bias. We choose not to consider this sort of information since it is not directly related to lensing. Furthermore for the small changes in n_i^A that we will typically be considering, the sample variance between the observed n_i^A and that predicted by the underlying redshift distribution and the photo-z parameters cannot be ignored (Hu & Kravtsov 2003). Therefore we will consider the number weighted power spectra $n_i^A n_j^A P_{ij}^\kappa$ as the fundamental lensing observables.

2.4. Fisher Matrix

The Fisher matrix quantifies the information contained in the lensing observables

$$O_{a=i(i-1)/2+j}(\ell) = n_i^A n_j^A P_{ij}^\kappa(\ell), \quad (i \geq j) \qquad (11)$$

on a set of cosmological and photo-z parameters p_μ. Under the approximation that the shear fields are Gaussian out to ℓ_{max}, the Fisher matrix is given by

$$F_{\mu\nu} = \sum_{\ell=2}^{\ell_{max}} (2\ell+1) f_{sky} \sum_{ab} \frac{\partial O_a}{\partial p_\mu} [\mathbf{C}^{-1}]_{ab} \frac{\partial O_b}{\partial p_\nu}, \qquad (12)$$

so that the errors on the parameters are given by $\Delta p_\mu = [\mathbf{F}^{-1}]_{\mu\mu}^{1/2}$.

Given shot and Gaussian sample variance, the covariance matrix of the observables becomes

$$C_{ab} = n_i^A n_j^A n_k^A n_l^A \left(P_{ik}^{tot} P_{jl}^{tot} + P_{il}^{tot} P_{jk}^{tot} \right), \qquad (13)$$

where $a = i(i-1)/2 + j$, $b = k(k-1)/2 + l$. The total power spectrum is given by

$$P_{ij}^{tot} = P_{ij}^\kappa + \delta_{ij} \frac{\gamma_{int}^2}{n_i^A}, \qquad (14)$$

where γ_{int} is the rms shear error per galaxy per component contributed by intrinsic ellipticity and measurement error. For illustrative purposes we will use $\ell_{max} = 3000$, f_{sky} corresponding to 4000 sq. deg., $\bar{n}^A$ corresponding to 55 galaxies/arcmin^2 and $\gamma_{int} = 0.4$.

For the cosmological parameters, we consider four parameters that affect the matter power spectrum: the physical matter density $\Omega_m h^2 (= 0.14)$, physical baryon density $\Omega_b h^2 (= 0.024)$, tilt $n_s (= 1)$, and the amplitude $\delta_\zeta (= 5.07 \times 10^{-5}$; or $A = 0.933$ Spergel et al. (2003)). Values in parentheses are those of the fiducial model. Unless otherwise stated, we shall take priors on these four parameters of $\Delta \ln \Omega_m h^2 = \Delta \ln \Omega_b h^2 = \Delta \ln \delta_\zeta = \Delta n_s = 0.05$. These priors represent only a modest improvement over current determinations. Our results on the relative degradation in constraints caused by photo-z errors are insensitive to reasonable variations in this choice.

To these four cosmological parameters, we add either two or three dark energy parameters: the dark energy density $\Omega_{DE} (= 0.73)$, its equation of state today $w_0 = p_{DE}/\rho_{DE}|_{z=0} (= -1)$ and optionally its derivative $w_a = -dw/da|_{z=0} (= 0)$ assuming a linear evolution with the scale factor $w = w_0 + (1-a)w_a$.

Note that throughout this paper, our notational convention is latin indices for tomographic bins and greek indices for parameters.

3. DARK ENERGY INFORMATION LOSS

In this section we consider the nature of the tomographic information on the dark energy and its loss to photo-z uncertainties. We establish the maximal information that can be gained through tomographic redshift divisions for a given dark energy parametrization. We then determine the number of photo-z degrees of freedom that would be required to lose this information. This loss of information is caused by a degeneracy between cosmological and photo-z parameters. We explicitly construct an example of this degeneracy as both an illustration and test of our statistical methodology.
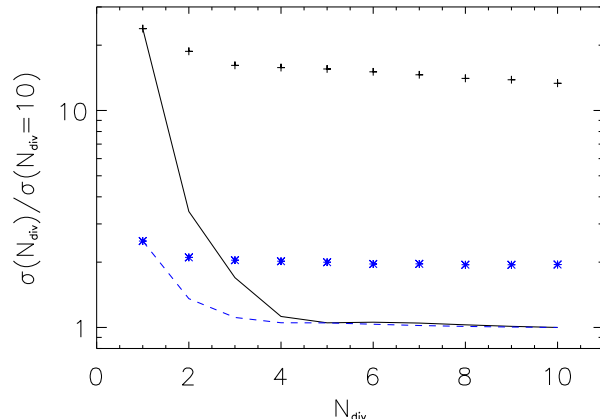

FIG. 3.— Relative errors in dark energy parameters as a function of the number of tomographic divisions N_{div}. Solid lines correspond to w_a for the set $\{w_0, w_a, \Omega_{DE}\}$; dashed lines to w_0 for $\{w_0, \Omega_{DE}\}$. Both lines assume that all photo-z parameters are perfectly known (i.e. fixed). Note that the results converge at smaller N_{div} for a smaller dark energy space, and that $N_{div} = 5$ is more than sufficient in either case. The points correspond to the same cases, but now with $2N_{pz} = 62$ photo-z parameters marginalized (with no prior information on them). Here essentially all tomographic information is lost so that the errors are comparable to those of $N_{div} = 1$ or no tomography.

TABLE 1
BASELINE CONSTRAINTS ON DARK ENERGY PARAMETERS

Photo-z Model	Parameters	$\sigma(\Omega_{DE})$	$\sigma(w_0)$	$\sigma(w_a)$
I	$\{\Omega_{DE}, w_0\}$	0.0062	0.061	-
	$\{\Omega_{DE}, w_0, w_a\}$	0.024	0.25	0.69
II	$\{\Omega_{DE}, w_0\}$	0.0073	0.070	-
	$\{\Omega_{DE}, w_0, w_a\}$	0.034	0.36	0.96

3.1. Maximal Information and N_{div}

For any given choice of dark energy parameterization, the information contained in lensing will saturate with some finite number of tomographic bins N_{div} (Hu 1999). Since the broad lensing kernel of equation (9) makes the shear for neighboring source redshifts highly correlated, most of the information is contained in a few coarse bins. The exact number depends on the type of information that is to be extracted. Roughly speaking, the number of bins should exceed the number of dark energy parameters.

Figure 3 (lines) quantifies this expectation through improvement in the errors on dark energy parameters as a function of N_{div} for Model I. For a 2 parameter dark energy space $\{w_0, \Omega_{DE}\}$, $N_{div} = 3$ divisions equally spaced from $z = 0$ to $z = 3$ are enough for the improvements in w_0 to saturate. For a 3 parameter dark energy space $\{w_0, w_a, \Omega_{DE}\}$, $N_{div} = 4$ divisions are sufficient for w_a. Note that $N_{div} = 1$ corresponds to no tomography or no photo-z information on the individual galaxies. The dark energy parameters that are not shown in Figure 3 behave similarly. In what follows we conservatively adopt $N_{div} = 5$ as sufficient to extract the dark energy information. With $N_{div} = 5$ and photo-z parameters fixed, the constraints on dark energy parameters are shown in Table 1.

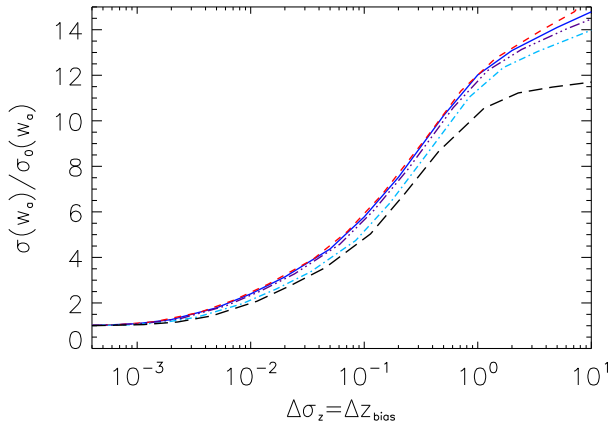Note that improvements relative to the no-tomography

FIG. 4.— Error degradations in w_a (that is, errors in w_a relative to the error with perfect knowledge of photo-z parameters) as a function of the photo-z prior. The photo-z priors are rescaled by a factor of $\sqrt{N_{\rm pz}/31}$ so that they reflect constraints per $\delta z = 0.1$ independently of $N_{\rm pz}$. Different lines from top to bottom correspond to different $N_{\rm pz}$: 61 (short dashed line), 31 (solid line), 21 (dash 3-dotted line), 11 (dash dotted line) and 6 (long dashed line). Note that the results have converged with $N_{\rm pz} \geq 21$; we use $N_{\rm pz} = 31$ just to be conservative.

case are more significant in the larger parameter space. This is due to the fact that w_0 is nearly degenerate with w_a since lensing mainly constrains $w(z)$ at some intermediate redshift (see below). Even the small amount of information in the fine-binned tomography assists the breaking of the degeneracy.

3.2. Maximal Degradation and $N_{\rm pz}$

Next we choose the number of photo-z parameters $N_{\rm pz}$ that describe each of the functions $z_{\rm bias}(z)$ and $\sigma_z(z)$. We seek to allow enough freedom in the photo-z parameters so that in the absence of prior information on their values all of the tomographic information is lost. Because the limit of no tomographic information corresponds to $N_{\rm div} = 1$, we have a quantitative means of assessing the minimal $N_{\rm pz}$. When $N_{\rm pz}$ becomes large enough, the variations in redshift, which act on the characteristic scale of $\delta z = 3.0/(N_{\rm pz} - 1)$, are rapid enough that they do not mimic any variation in cosmological parameters.

Figure 4 shows the degradation in the errors on w_a for the cases of $N_{\rm pz} = 6$, 11, 21, 31 and 61 as a function of the prior on the photo-z parameters. Results for w_0 are similar. To compare priors for different $N_{\rm pz}$ values, we have here rescaled the individual parameter priors by $\sqrt{N_{\rm pz}/31}$ so as to be equal for a fixed redshift interval $\delta z = 0.1$. The results have converged with $N_{\rm pz} \geq 21$. To be conservative, in the rest of this paper we use $N_{\rm pz} = 31$, or a total of 62 photo-z parameters.

The impact of this choice of $N_{\rm pz} = 31$ as a function of $N_{\rm div}$ for w_0 is shown in Figure 3 (points). For all $N_{\rm div}$, these constraints match those with no tomographic binning very well, showing that without prior information on the photo-z parameters all tomographic information has been effectively destroyed and we recover the case with a single redshift division. The small discrepancy comes from the fact that the Fisher matrix is a local approximation to the parameter errors as we shall discuss in the next section.

3.3. Photo-z – Dark Energy Degeneracy

With a sufficient number of unknown photo-z parameters $2N_{\rm pz} \gtrsim 62$, the Fisher matrix results of the previous section imply that dark energy information in tomography is completely lost. This fact implies that there is a nearly perfect degeneracy between photo-z, dark energy and other cosmological parameters. Here we examine that aspect of the degeneracy that involves the photo-z and dark energy parameters only. This degeneracy alone suffices to destroy most of the tomographic information and will remain even if the other cosmological parameters are perfectly measured from other sources.

Constructed from parameter derivatives, the Fisher matrix is a local expression of the degeneracy in parameter space. Because the Fisher matrix results imply that the degeneracy persists to large changes in the dark energy parameters, it is important to assess the extent of the degeneracy more directly and test the validity of the Fisher approximation. If the degeneracy relation "curves" in parameter space, the Fisher approximation will only find the local tangent.

We start by identifying this local tangent with the Fisher matrix. To isolate the degeneracy between dark energy and photo-z parameters, we eliminate the other cosmological parameters, formally by adding strong priors to the Fisher matrix. For numerical reasons we also add a weak prior on photo-z parameters ($\Delta z_{\rm bias} = \Delta \sigma_z = 1$) to control numerical errors from the nearly singular Fisher matrix. Of the eigenvectors of this Fisher matrix that involve the dark energy, those with the smallest eigenvalues will be responsible for most of the photo-z dark energy degeneracy. We find that a single linear combination of parameters (dark energy *and* photo-z) contributes most ($\sim 98\%$) of the errors in dark energy parameters w_0 and w_a. Thus the degeneracy is essentially one dimensional in the multi-dimensional parameter space. Let us call this direction – or the eigenvector of the Fisher matrix – $\mathbf{e}_w$.

The true extent of the degeneracy is quantified by the change in χ^2 between the fiducial model p_μ and a trial model $\tilde{p}_\mu$

$$\Delta \chi^2_{\rm true} = \sum_{\ell=2}^{\ell_{\rm max}} (2\ell + 1) f_{\rm sky} \sum_{ab} [O_a(\ell; p_\mu) - O_a(\ell; \tilde{p}_\mu)]$$
$$\times [\mathbf{C}^{-1}]_{ab} [O_b(\ell; p_\mu) - O_b(\ell; \tilde{p}_\mu)] . \qquad (15)$$

If the Fisher matrix approximation were valid out to say 1σ along the degeneracy then the trial model $\tilde{p}_\mu = p_\mu + \sigma_w \mathbf{e}_w$, where σ_w^{-2} is the eigenvalue corresponding to $\mathbf{e}_w$, would be separated by

$$\Delta \chi^2_{\rm F} = \sigma_w^2 \mathbf{e}_w^T \mathbf{F} \, \mathbf{e}_w = 1 \qquad (16)$$

due to the orthonormality of the eigenvectors. In practice $\Delta \chi^2_{\rm true} = 857$ for this extrapolation indicating a curvature in the degeneracy direction. In other words, p_μ and $\tilde{p}_\mu$ are highly distinguishable models in spite of the Fisher predication that they are indistinguishable.

Even given curvature in the degeneracy direction, the Fisher approximation remains useful if it accurately predicts the extent of the degeneracy. This is especially true if the curvature lies mainly in the photo-z nuisance parameters which exist only to be marginalized. To assess the extent of the degeneracy, we use the Fisher matrix as

a local approximation of the degeneracy with the following procedure. Starting at the fiducial model, calculate the Fisher matrix and find $\mathbf{e}_w$ as defined above, then take a *small* step along $\mathbf{e}_w$ direction. Now calculate the Fisher matrix at the new point, find the new $\mathbf{e}_w$, take another small step along this new direction. Repeat.
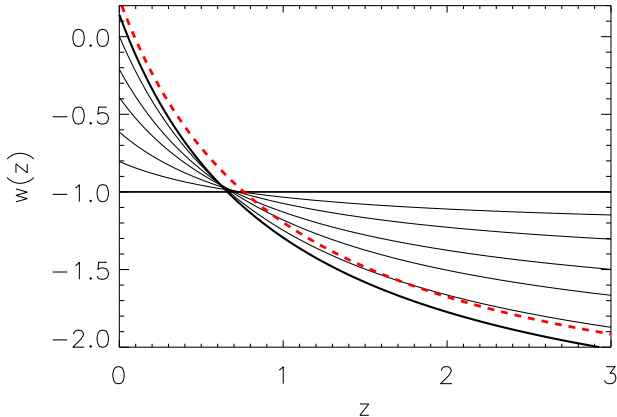

FIG. 5.— Equations of state of dark energy $w(z)$ that are degenerate with photo-z parameters. Solid lines show a series of degenerate models stepping out by $\Delta w_0 = 0.2$ and ending at a model with $\Delta w_0 = 1.14$ which deviates from the fiducial model at $+1\sigma$ for the fiducial survey. The tight correlation between w_0 and w_a along the degeneracy direction results in the tight "waist" or pivot where $w(z)$ remains well determined. The dashed line shows that the $+1\sigma$ degenerate model as predicted by the Fisher matrix is in good agreement with the true degeneracy even out to large Δw_0.

From this construction we find that the extent of the degeneracy in w is accurately predicted by the Fisher matrix. Figure 5 shows that the model with $\Delta \chi^2_{\rm F} = 1$ (thick dashed line) is almost identical to the model with $\Delta \chi^2_{\rm true} = 1$ (thick solid line) in $w(z)$. In Figure 5 we also show intermediate models along the degeneracy with $\Delta \chi^2_{\rm true} < 1$. That they all pass through essentially a single point in $w(z)$ space is another indication that the degenerate direction thus lies almost entirely along a specific linear combination of dark energy parameters as predicted by the Fisher matrix. The curvature in parameter space involves the photo-z parameters.

The redshift at which these curves intersect is $z \approx 0.7$ and at this redshift measurements of w are essentially immune to photometric redshift errors. This immunity reflects the fact that even without tomography lensing can constrain the equation of state at some effective redshift. With two parameters to describe $w(z)$, there is only one remaining linear combination to be affected by photometric redshifts. With a more general parameterization of $w(z)$ we expect that there will be multiple degenerate directions with roughly the same single aspect of $w(z)$ preserved.

Furthermore, the two estimates (true and Fisher) agree on the amplitude of the photo-z parameter variation along the degenerate direction. For example, at a point along the $\mathbf{e}_w$ direction which is 1σ away from the fiducial model, the Fisher matrix indicates that the photo-z parameters changed by $\delta z_{\rm bias} < 0.06$ and $\delta \sigma_z < 0.06$, while the actual bounds on the variations are $\delta z_{\rm bias} < 0.04$ and $\delta \sigma_z < 0.04$. Note that these changes are fairly small and imply that subtle variations in the redshift distributions
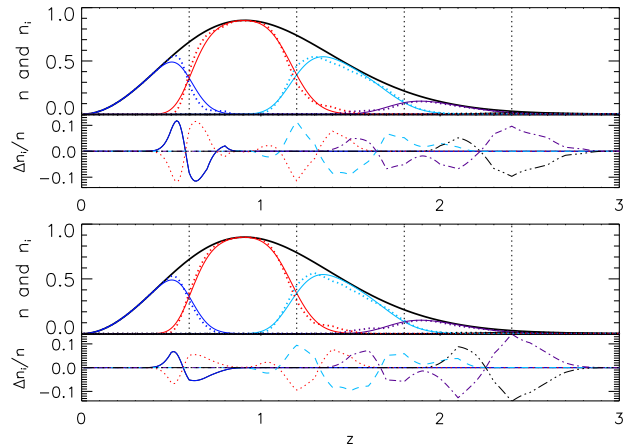

FIG. 6.— Comparison of the $n_i(z)$ of tomographic bins for two models that are separated by 1σ. Bottom panel shows the fiducial model (solid curves) and the model that is 1σ away (dotted lines) as predicted by the Fisher matrix. Top panel shows the same, except the latter model is now obtained by following the actual degeneracy direction (rather than approximating it using the Fisher matrix). Within each panel the upper plot shows the fiducial (Model I) and 1σ-degenerate tomographic distributions of galaxies while the lower plot shows the relative differences between the two.

for the tomographic bins are responsible for a degeneracy that degrades errors in w_0 and w_a by an order of magnitude. Figure 6 shows that the difference between these distributions for $\Delta \chi^2_{\rm true} = 1$. We expect that with a change in the photo-z model, the specific photo-z variations that establish this degeneracy will change but that a strong degeneracy will remain.

In summary, we find that the Fisher matrix is an adequate tool for assessing the existence and extent of degeneracies between photo-z and dark energy parameters. It should not however be used to infer the specific changes in the photo-z parameters that establish the degeneracy.

4. PHOTO-Z INFORMATION RECOVERY

In the previous section, we established the existence of a degeneracy between photo-z parameters and dark energy parameters and tested the validity of the local Fisher matrix approximation to this degeneracy. In this section, we use the Fisher matrix formalism to investigate the extent to which prior information on the photo-z distributions help recover the tomographic dark energy information. We assume $2N_{\rm pz} = 62$ photo-z parameters and $N_{\rm div} = 5$ tomographic bins through out this section (see §3).

4.1. *Photo-z Priors*

We now explore the effect on dark energy parameter constraints of priors on each of the photo-z parameters $z_{\rm bias}(z_\mu)$ and $\sigma_z(z_\mu)$. For simplicity, we begin by applying a redshift independent prior on the parameters. In practice parameters controlling the distributions well above and well below the median redshift require weaker priors. We will discuss this point in §4.3.

In Figure 7, the left panel shows the error degradation in w_0 assuming the $\{w_0, \Omega_{\rm DE}\}$ parametrization (left panel) and w_a assuming the $\{w_0, w_a, \Omega_{\rm DE}\}$ parametrization (right panel). For reference the baseline errors for the fiducial survey are listed in Table 1.

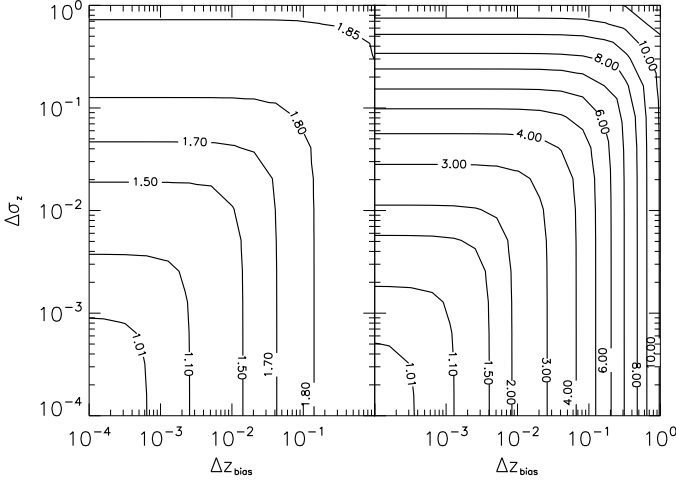FIG. 7.— Error degradations in constant w_0 (left panel) and those in w_a when where both w_0 and w_a are varied (right panel), as a function of photo-z parameter priors. Here the degradations are defined as actual errors relative to errors that assume the photo-z parameters to be perfectly known. Priors on the photo-z parameters $z_{\mathrm{bias}}(z_\mu)$ and $\sigma_z(z_\mu)$ are shown on the x-axis and y-axis respectively. Fiducial photo-z model I is assumed and the photo-z parameter spacing in redshift is $\delta z = 0.1$.

As in the previous section where other cosmological parameters were artificially fixed, we find that the larger dark energy parameter space is more susceptible to photo-z errors. For example, for the extreme case of no photo-z information, i.e. very weak priors on both bias and scatter parameters, dark energy parameters of the $\{w_0, \Omega_{\mathrm{DE}}\}$ parameterization are degraded by about a factor of two while those of $\{w_0, w_a, \Omega_{\mathrm{DE}}\}$ parameterization are degraded by about a factor of ten.

In the more relevant case where we demand that the dark energy error degradation be no larger than 1.5, the requirement per photo-z parameter is about 0.01 for $\{w_0, \Omega_{\mathrm{DE}}\}$ and 0.003 for the $\{w_0, w_a, \Omega_{\mathrm{DE}}\}$ parametrization. Figure 7 also shows that both bias and scatter parameters are important, and that knowledge of the bias is only slightly more important than that of the scatter. Furthermore, dark energy parameters that are not shown in Figure 7 have very similar requirements to those plotted in either parametrization.

4.2. Dependence on Fiducial Model

The results above are for a specific choice of the fiducial model for the photo-z distribution and survey. To explore the dependence on the former we take the very different photo-z Model II, where the scatter is substantially larger and jumps discontinuously in redshift. Even so the requirements on the photo-z parameters are very similar; see Figure 8. In particular, within the interesting regime where the photo-z prior is smaller than unity and the degradation in dark energy parameter errors is a factor of a few or lower, the two models agree very well.

On the other hand, photo-z requirements do depend on the parameters f_{sky}, γ_{int} and n^A that determine the level of sample and noise variance in the survey. The trend is that the more ambitious the survey, the more stringent the requirements on photo-z parameters. The scaling for the priors on photo-z parameters can roughly

be described as

$$\frac{\Delta p(f_{\mathrm{sky}}, \gamma_{\mathrm{int}}, n^A, d)}{\Delta p(0.1, 0.4, 55, 1.5)} = \frac{g(d)}{g(1.5)}\sqrt{\frac{0.1}{f_{\mathrm{sky}}}} \qquad (17)$$

$$\times \left[1 + C\left(\frac{\gamma_{\mathrm{int}}^2}{0.16}\frac{55}{n^A} - 1 \right) \right],$$

where $\Delta p = \Delta z_{\mathrm{bias}} = \Delta \sigma_z$ gives the photo-z priors and n^A is in units of arcmin^{-2}. Here $g(d) = \Delta p(0.1, 0.4, 55, d)$ scales the prior requirement to alternate levels of degradation d; it is shown in Figure 8 as $d(g)$ and is only weakly dependent on the fiducial photo-z model. With the best fit $C = 0.6$ this scaling is good up to a factor of 2 for any reasonable set of survey parameters.

Finally the photo-z precision requirement is not very sensitive to z_s, the median source redshift of the survey. For $0.68 < z_s < 1.3$, Δp varies by less than 40%.
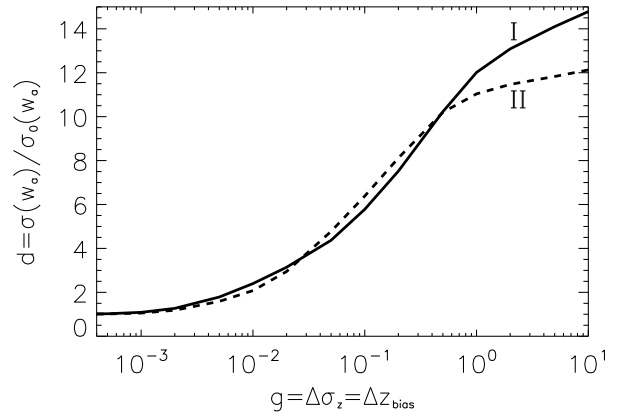

FIG. 8.— Comparison of the photo-z requirements for our two fiducial photo-z models. The solid line shows the degradations for model I while the dashed line corresponds to model II. The fiducial errors in w_a when the photo-z's are perfectly known are $\sigma_0(w_a) = 0.69$ (model I) and $\sigma_0(w_a) = 0.96$ (model II).

4.3. Training Set Size

The priors on the photo-z parameters ultimately require a training set of galaxies with measured spectroscopic redshifts. Operationally suppose that a photo-z training set has N_{spec}^μ spectroscopic redshifts per redshift interval determined by N_{pz} (here $\delta z = 0.1$).

Given a Gaussian distribution for the photo-z distribution and a fair sample of spectroscopic galaxies selected from this distribution, the training set would independently determine the bias and scatter to

$$\Delta z_{\mathrm{bias}}(z_\mu) = \sigma_z(z_\mu)\sqrt{1/N_{\mathrm{spec}}^\mu} \,,$$

$$\Delta \sigma_z(z_\mu) = \sigma_z(z_\mu)\sqrt{2/N_{\mathrm{spec}}^\mu} \,. \qquad (18)$$

For a fixed dark energy degradation, N_{spec}^μ depends on two things: the fiducial σ_z and the required prior as scaled from equation (17). Since the photo-z prior requirement is roughly independent of σ_z as shown in Figure 8, the larger the scatter, the larger the required training set. Note that N_{spec} ($\equiv \sum_\mu N_{\mathrm{spec}}^\mu$) is robust to changes in the number of photo-z parameters or δz. For

example a binning of $\delta z = 0.05$ would imply twice as many photo-z parameters that would need to be constrained a factor of $\sqrt{2}$ less well, yielding the same requirement on $N_{\rm spec}$.

For determining the redshift extent of the training set, it is important to go beyond our simple redshift independent prior. Figure 10 shows the cumulative $N_{\rm spec}(> z)$ required for 1.5 degradation in dark energy. Notice that this flat prior assumption would require a substantial number of galaxies across the whole redshift range (10^5), including 8×10^4 galaxies above $z = 1.5$. This number is artificially high since the actual requirements on the prior fall sharply away from the median redshift of the distribution.

To illustrate the difference, we constructed a weighted template of how the bias and scatter priors vary with redshift to produce a fixed degradation in dark energy parameters. We choose a simple power law of $\bar{n}_i$ which is the number of galaxies in each redshift interval ($\delta z = 0.1$ for the fiducial choice of $N_{\rm pz} = 31$) corresponding to the photo-z parameters. At $z < 1.2$, the power is chosen as -1. To account for the difficulty in measuring redshifts at $z > 1.5$ from optical bands, we steepen the index to -3 for $z > 1.2$. Figure 9 compares the flat prior to the weighted one. The requirement for the weighted one

FIG. 10.— Cumulative requirement of $N_{\rm spec}$ for 1.5 dark energy error degradation. The corresponding photo-z prior templates are shown in Figure 9 with (1; dashed) as the flat prior and (2; solid) as the weighted prior.

FIG. 11.— The ratio of required $N_{\rm spec}$ for an arbitrary w_a degradation relative to that of 1.5 degradation for the two prior templates of Figure 9.
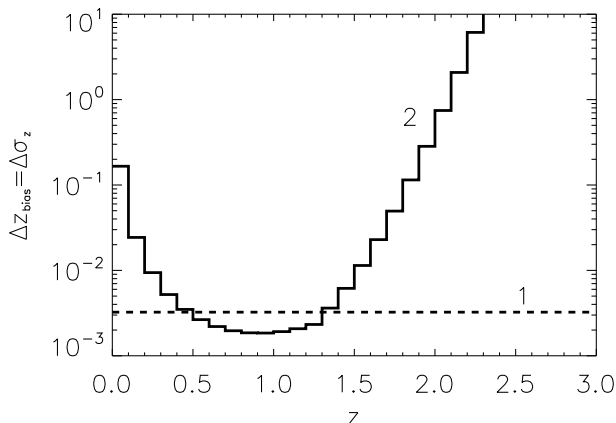

FIG. 9.— Photo-z prior templates of how the bias and scatter priors vary with redshift to produce a fixed error degradation in dark energy parameters. The degradation on w_a is 1.5. The straight line (1; dashed) is the flat template used in Figure 7. The curved line (2; solid) is the weighted template constructed according to the galaxy number density. At $z < 1.2$, the curve follows $\bar{n}_i^{-1}$ while at $z > 1.2$, the curve follows $\bar{n}_i^{-3}$. Here $\bar{n}_i$ is the number of galaxies in each redshift interval $\delta z = 0.1$.

drops to a total of 4×10^4 but more importantly only 300 at $z > 1.5$.

For dark energy degradations other than 1.5, we provide in Figure 11 the ratio of $N_{\rm spec}$ for an arbitrary dark energy degradation to that of 1.5 degradation. In order to find out the $N_{\rm spec}$ requirement for any dark energy degradation, all one needs to do is to look up the ratio in Figure 11 and multiply it by the $N_{\rm spec}$ in Figure 10.

We have tested that the scaling relation to surveys with different fiducial parameters of equation (17) works equally well for both the flat and weighted priors. Using the scaling relation, the requirement of $N_{\rm spec}$ could be scaled to different survey easily.
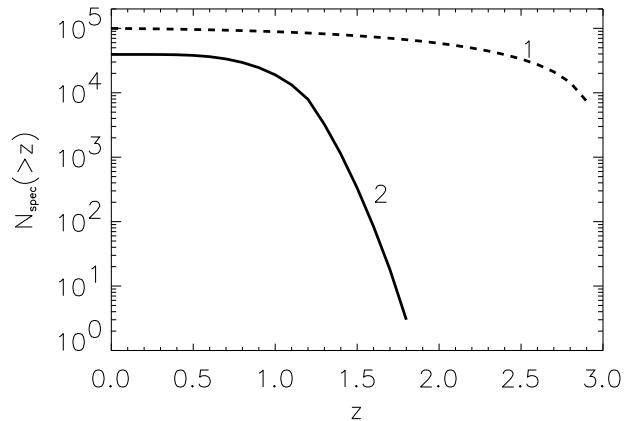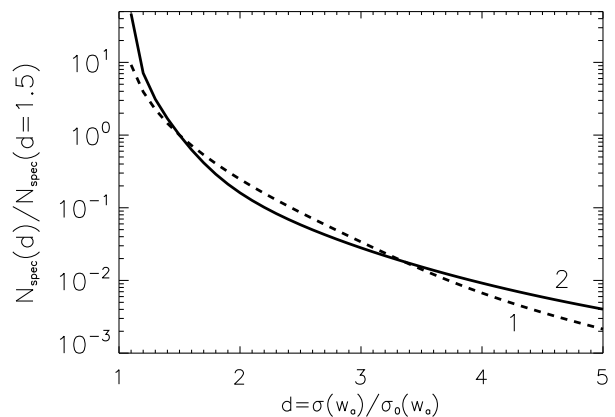
4.4. Mean vs. Median

We now estimate the amount of information that comes from knowing the median or mean of the redshift distribution of source galaxies in each tomographic bin. Note that this is distinct from priors on the photo-z bias or mean photo-z at a given redshift. This question is interesting in its own right, but also because other work, parallel to this (Huterer et al. 2005) has parametrized the photo-z uncertainty by the centroids of the tomographic bins, which when varied shift the overall distribution of the corresponding tomographic bin. While one intuitively expects that the centroid of the photo-z bin (or, more generally its mean) carries the most information, we now have the tools to precisely examine the relative contribution of the mean relative to that of the higher moments.

Figure 12 shows degradations of the error in w_a as a function of priors on the mean or median of the tomographic bins. All of the photo-z parameters are given a weak prior of unity for numerical stability. A prior of 10^{-3} on the mean is enough to render the mean essentially precisely known. But the dark energy degradation is still a factor of 2 even with perfect mean measurements
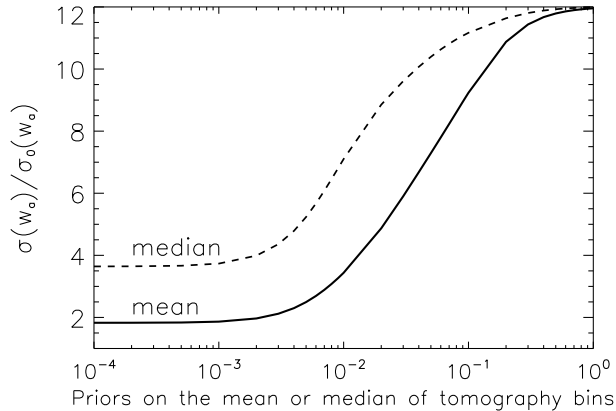
FIG. 12.— The effect of the mean or median of tomography bins. Vertical axis is dark energy error degradation. The solid line and the dashed line are for the case of mean and median respectively. Photo-z priors of $\Delta\sigma_z = \Delta z_{\mathrm{bias}} = 1$ are assumed.

showing that there remains information lost to the higher moments of the distribution.

Similarly, while the mean of the tomographic distribution does carry the majority of the information, the median carries significantly less (see Figure 12). The reason is that the mean has extra information about the tails of the redshift space distribution while the median does not. This sensitivity to the tails will make obtaining precise measurements of the mean difficult. One still requires a fair sample from each of the tomographic redshift bins extending to high redshift. In the end, mean priors require a similar number of training set galaxies as above.

5. DISCUSSION

We have performed a general study of the effects of imperfect photometric redshifts on weak lensing tomography. Describing the photo-z distribution with a bias and scatter that is an arbitrary function of redshift, we studied the degeneracies between photo-z and dark energy parameters, as well as the resulting degradations in dark energy parameter errors.

Not surprisingly, we find that there exist significant degeneracies between the dark energy and photo-z parameters. Assuming that the overall distribution of galaxies $n(z)$ is independently known and the photometric redshifts are used only for tomographic subdivision, we find that larger dark energy spaces suffer more degeneracy with photo-z than the smaller ones.

Without any information on photo-z parameters, one recovers the no tomography case where errors on fiducial parameters are a factor of two times worse (for the $\{w_0, \Omega_{\mathrm{DE}}\}$ parametrization) or ten times worse (for the $\{w_0, w_a, \Omega_{\mathrm{DE}}\}$ parametrization) than those for the 10-bin tomography case with perfect photo-z's.

For the fiducial survey, in order to have less than a factor of 1.5 degradation in dark energy parameter errors, the photo-z parameters z_{bias} and σ_z (defined in the redshift interval $\delta z = 0.1$) should each be controlled to better than 0.003-0.01, depending again on the size of dark energy parameter space. We provide a convenient approximation for scaling these requirements to different surveys. Importantly, no single number such as the mean or median of galaxies in the tomographic bin captures all of the effect of photo-z errors. That the mean captures more of the information than the median indicates that the dark energy information is sensitive to the tails of the distribution.

In order to achieve less than a factor of 1.5 degradation in the evolution of the equation of state, a training set of a few times 10^4 galaxies with spectroscopic redshifts is required. Again, one can easily rescale the number of galaxy requirement to different surveys using our scaling relation.

There are several caveats to our assessment that merit future study. Although our parametrization can handle photo-z degeneracies that lead to bimodality and catastrophic errors, we have limited our study to fiducial models around which their effects are small. Moreover, we have assumed that the parent redshift distribution of the survey is known and that photometric redshifts are only employed to subdivide the galaxy sample for tomography. Uncertainties in the parent distribution can further degrade dark energy determinations.

On the other hand, uncertainties in the parent distribution are also constrained by the training set. If one assumes that $n(z)$ is a smooth function that is parametrized by relatively few parameters, uncertainties in the parent distribution should be smaller than those of the tomographic bins. For illustrative purposes, if we parametrize $n(z)$ with the three parameters of equation (2), we find that the constraint on $n(z)$ from N^{μ}_{spect} is good enough to have dark energy parameter errors differ by less than 10% from the case where $n(z)$ is fixed.

Given the current state-of-the-art of photo-z algorithms as well as expected improvements with multiwavelength observations of all source galaxies, prospects for sufficiently accurate determination of photometric redshifts are bright. Nevertheless, it will be an important and challenging task to achieve good control of the photo-z accuracy for the specific types of galaxies selected in lensing surveys, and then propagate the remaining photo-z errors into the final cosmological constraints.

REFERENCES

Aldering, G. et al. 2004, PASP, submitted (astro-ph/0405232)
Bacon, D. J., Refregier, A. R., & Ellis, R. S. 2000, MNRAS, 318, 625
Bartelmann, M., & Schneider, P. 2001, Physics Reports, 340, 291

Bernstein, G. & Jarvis, B. 2002, AJ, 583, 123
Brown, M.L., Taylor, A.N., Bacon, D.J., Gray, M.E., Dye, S., Meisenheimer, K. & Wolf, C. 2003, MNRAS, 341, 100
Bunn, E. F., & White, M. 1997, ApJ, 480, 6

Cooray, A., & Hu, W. 2000, ApJ, 554, 56

Cunha, C. E., Oyaizu, H., Lima, M. V., Lin, H., Frieman, J., et al. 2005, in preparation

Dodelson, S. & Zhang, P. 2005, astro-ph/0501063

Eisenstein, D.J. & Hu, W. 1999, ApJ, 511, 5

Eisenstein, D. J., Hu, W., & Tegmark, M. 1999, ApJ, 518, 2

Hagan, B., Ma C-P. & Kravtsov A. 2005, astro-ph/0504557

Heitmann, K., Ricker, P. M., Warren, M. S., Habib, S., 2004, astro-ph/0411795

Heymans, C. et al. 2005, astro-ph/0411324

Hirata, C. & Seljak, U. 2003, MNRAS, 343, 459

Hoekstra, H. 2004, MNRAS, 347, 1337

Hoekstra, H., Yee, H. & Gladders, M. 2002, ApJ, 577, 595

Hu, W. 1999, ApJ, 522, L21

Hu, W. 2002, Phys. Rev. D, 65, 023003

Hu, W. 2003, Phys. Rev. D, 66, 083515

Hu, W., & Kravtsov, A. 2003, ApJ, 584, 702

Hu, W., & Tegmark, M. 1999, ApJ, 514, L65

Huterer, D. & Takada, M. 2005, Astropart. Phys., 23, 369

Huterer, D., Takada, M., Bernstein, G & Jain, B. 2005, astro-ph/0506030

Huterer, D., & White, M. 2005, astro-ph/0501451

Huterer, D., 2002, Phys. Rev. D, 65, 063001

Ishak, M. 2005, astro-ph/0501594

Jarvis, M., Bernstein, G., Jain, B., Fischer, P., Smith, D., Tyson, J.A. & Wittman, D. 2003, AJ, 125, 1014

Jarvis, M., Jain, B., Bernstein, G. & Dolney, D. 2005, astro/ph/0502243

Jarvis, M. & Jain, B. 2004, astro-ph/0412234

Kaiser, N. 1992, ApJ, 388, 272

Kaiser, N. 1998, ApJ, 498, 26

Kaiser, N., Wilson, G., & Luppino, G. A. 2000, astro-ph/0003338

Peacock, J.A. & Dodds, S.J. 1996, MNRAS, 280, L19

Pen, U.-L., van Waerbeke, Y. & Mellier, Y. 2002, ApJ, 561, 31

Pen, U.-L. et al. 2003, ApJ, 592, 664

Refregier, A. 2003, Ann. Rev. Astron. Astrophys., 41, 645

Refregier, A. et al. 2004, , AJ, 127, 3102

Rhodes, J., Refregier, A. & Groth, E. 2000, ApJ, 536, 79

Seljak, U. & Zaldarriaga, M. 1996, ApJ, 469, 437

Song, Y.-S. & Knox L. 2004, Phys. Rev. D, 70, 063510

Spergel, D.N. 2003, ApJ, 148, 175

Takada, M. & Jain, B. 2004, MNRAS, 348, 897

Takada, M. & White, M. 2004, ApJ, 601, L1

Vale, C. & White, M., 2003, ApJ, 592, 699

Vale, C., Hoekstra, H., van Waerbeke, L. & White, M. 2004, ApJ, 613, L1

Van Waerbeke, L. et al. 2000, A&A 358, 30

Van Waerbeke, L., Mellier, Y., 2003, astro-ph/0305089

Van Waerbeke, L., Mellier, Y. & Hoekstra, H. 2005, A&A 429, 75

White, M., 2004, Astroparticle. Phys., 22, 211

White, M., 2005, Astroparticle. Phys., 23, 349

White, M. & Hu, W., 2000, ApJ, 537, 1

White, M. & Vale, C., 2004, Astroparticle. Phys., 22, 19

Wittman, D., Tyson, J. A., Kirkman, D., Dell'Antonio, I., & Bernstein, G. 2000, Nature, 405, 143

Zhan, H. & Knox, L. 2004, ApJ, 616, L75